# Chapter 2 – FACILITIES AND METHODS

High rate, high amplitude motions are more readily studied in liquids (water, water/glycerin mixtures and the like) than in air [21]. The ratio of model inertia (the model's physical mass) to fluid-dynamic loads is much lower in liquids than in air, leading to improved signal-to-noise ratio. PIV particle seeding is also easier in the liquid phase [22].

## 2.1 AFRL

AFRL data were taken in the United States Air Force Research Lab, Aerospace Systems Directorate's water tunnel, by K.O. Granlund and M.V. Ol, and separately by P. Mancini and A. Jones, thus producing two data sets. The tunnel is of free-surface type, with test section 18" wide, 24" high and 96" long. Nominal turbulence intensity (measured by particle image velocimetry and laser-Doppler velocimetry) is 0.4% at 15 – 40 cm/s, and speed range is 3 – 90 cm/s. The tunnel is powered by a 16"-diameter axial impeller pump, flowing water through a vertical perforated distribution pipe into the intake plenum, a settling chamber with 3 screens and 2 honeycombs, and 3.8:1 contraction. The tunnel is fitted with three degree of freedom motion system, consisting of three linear electric servomotors and a proportional-integral-derivative programmable controller. Two motors vertically oriented above the test section actuate pitch and plunge with up to 8" stroke, while a third motor above the aft end of the test section has 48" stroke of fore-aft translation, or surge. All rectilinear motions are possible, other than continuous rotation in pitch (pitch is limited to 0° – 90° or ± 45°). Translational surging motions are via the horizontal motor, with the tunnel shut off, and the two vertical motors set to place the model at 45-degrees incidence. The model mounted horizontally in the test section, with a central support also housing the load cell. Translational pitch uses the same orientation. In the typical translational arrangement, the plate is mounted offset from the load cell by a 2.25" 3D-printed plastic strut Rotational surge uses all three motors, with the model hanging vertically from an arm offset from the load cell, with the load cell reference-center at the point of rotation.

The equipment suite includes:

- PCO Dimax 4Mpix 1279 frame-per-second, 12-bit CMOS camera, for PIV and flow visualization, typically mounted laterally from the test section.
- Photonix DM55 55 mJ/pulse 3 KHz single-cavity Nd:YLF laser, fired asynchronously for PIV, and synchronously for planar laser fluorescence for flow visualization by injection of dye from the plate leading/trailing edges.
- ATI NANO-25 and NANO-17 [23] 6-component load cells, triggered by the motion-rig, mounted in a frame connected to "plunge rods" from the two vertical linear motors.
- Positive-displacement syringe pump for adjustable-flow of dye (food coloring or rhodamine, the latter for planar laser fluorescence).

Photographs of the facility and typical models are shown in Figure 2-1. PIV is of the conventional 2D type, using Lavison's DaVis 8.1 software and the 5 μm Vestosint seeding particles. With a multi-pass, variable window-size method, the first pass used a 48 x 48 pixel window with 1:1 square weighting and 50% overlap, and two further passes used 32 x 32 pixel windows with 1:1 circular weighting and 75% overlap. Post-processing was kept to a minimum by only utilizing a remove-and-replace median filter of 2 standard deviations.

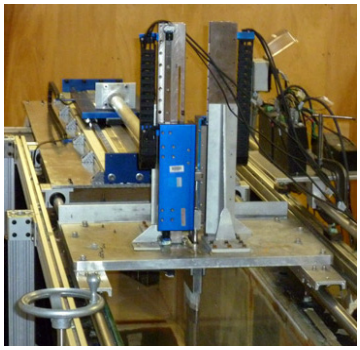

(a)

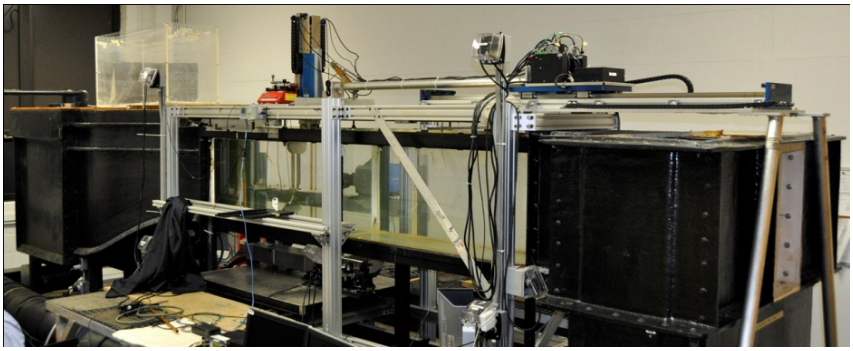

(b)

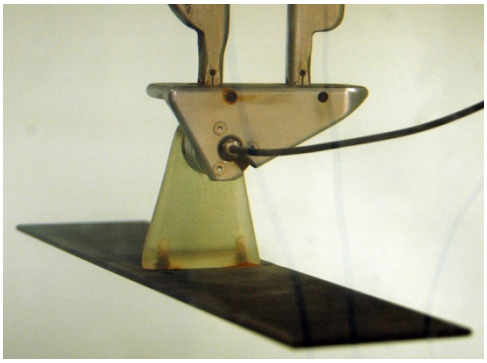

(c)

**Figure 2-1: AFRL Water Tunnel. Electric motion-rig, with a horizontal linear motor actuating in the streamwise direction a carriage with two vertical linear motors (a); the latter are responsible for pitch/plunge motions, and the former for surge. Overall view of water tunnel, from intake plenum to test section and exit plenum (b). AR = 4 plate installed for rectilinear motions (c).**

Processing/filtering of force-data is discussed in Granlund *et al*. [24], with low-pass filtering ultimately limited by the system natural frequency, typically at ~ 13 Hz (as determined by strike-test of the model) in post-processing, and at 18 Hz in the load-cell's native acquisition system, with sampling at 1 KHz.

For translations, the principal case was an AR = 4 carbon fiber plate with $c$ = 76.2 mm and thickness ~ 3 mm. Due to the length of the test section, maximum translation distance was limited to approximately 14 $c$ for the surge cases. A typical model installation is shown in lower part of Figure 2-1.

## 2.2 ARL

The U.S. Army Research Lab (ARL) group (K. Kroninger, M. Munson, A. Harrington and B. Cohen) used an oil tank for force/moment data on rotating wings. The hexagonal tank is 63.5 cm across and 76 cm tall) Figure 2-2, filled with mineral oil of 850 kg/m$^3$ density and 16.8 mPa-s viscosity at room temperature.

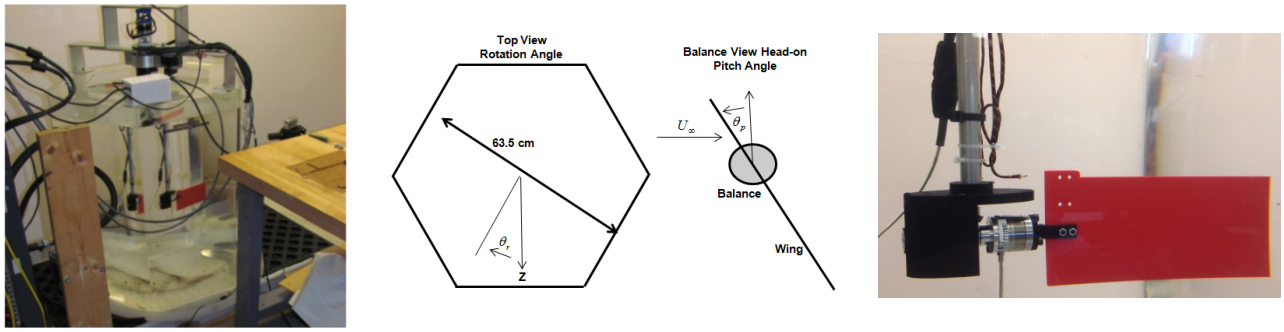


(a) (b) (c)

**Figure 2-2: The ARL Oil Tank Facility. (a) The hexagonal tank with supporting infrastructure; (b) The definition of the motion coordinate systems for the rotation and pitch degrees of freedom; and (c) The wing model mounted on the wing mid-chord in a vertical orientation.**

The model is supported on a six component balance, with the axis of rotation for the wing in the center of the tank. Rotation is controlled by a stepper motor from the top of the tank, with the motion transmitted down the larger of two concentric shafts. The mechanics for the wing pitching motion are mounted in the rotating frame of reference with a second stepper motor controlling the wing pitch through the center shaft. Utilizing micro-stepping, a resolution of 2000 steps per revolution was achieved. Both axes of motion have a gear down ratio from the motor to the axis of rotation, resulting in positioning resolutions of 10,000 and 4000 steps per revolution in the rotation and pitch axes, respectively. From visual inspection, it is estimated that +/-1.5° of alignment accuracy can be achieved, plus another +/1.5° of backlash. The model, depicted in Figure 2-2(c), has AR = 2 (based on the semi-span and area), a rectangular planform, 15.2 cm by 7.6 cm and a thickness of 3.7 mm. It is designed to reside a half chord length from the axis of rotation. The wing tip is about 5/3 chords from the tank wall at the closest points in the rotation, so a small influence from the presence of the wall might be anticipated.

Two sets of wing kinematics were explored. One is rotation at a pitch angle of 45° (Figure 2-2), with a surging start. The acceleration for the surging start is completed in about two chord lengths following the profile of a smoothed quadratic polynomial spline for the commanded acceleration. The second is a pitch-up from a pitch angle of 90° to 45° while already rotating. The pitch-up is completed within the first revolution of the wing over 8 chord lengths of travel. The wing displacement over time is described by the Eldredge smoothing function [7] with a value of 0.05 for the reduced frequency and 11 for the smoothing parameter. The distance travelled is measured at the ¾ span location for both cases and 4 π chord lengths equals a revolution.

The forces and moments at the base of the wing are measured with a six component balance, with a range of +/- 500 N in its longitudinal axis (the wing's spanwise axis) and +/- 125 N in the lateral directions. The moment limits in all axes are 3 N-m. The measurement accuracy is described by the manufacturer to be better than 0.01% of the full-scale range for all axes [23]. Voltage supplied to the balance and the analog outputs is routed through a slip ring out of the rotational frame to a signal conditioning unit and ultimately to an Analog-to-Digital Converted (ADC). The angular motions of the rotational and pitch axes are each monitored with an optical quadrature encoder mounted on each motor.

The force and encoder signals were all measured simultaneously with a high-speed ADC, sampled at 51,200 Hz. The high-speed ADC applies a combination of a digital and analog filtering to prevent aliasing. The resulting filtering behavior is a low pass filter with a cut-off frequency that is one half the sample rate (the Nyquist

frequency) [25]. A zeroing process was performed just before and after each data collection run to account for balance drift and the model's weight. The force time histories were further filtered with a discrete truncated approximation of an ideal low pass filter. A 10 Hertz cut-off frequency, applied over a four second range centered around the current time step, was utilized for the convolution of the ideal filter impulse with the force time histories. The difference between the digitally filtered data and the original time history was used to form a moving standard deviation. The moving standard deviation is calculated from 100 ms of data, the period of the 10 Hz cut-off frequency. Error bars representing three standard deviations are plotted with the digitally filtered data reflecting a 99% percent confidence interval assuming a Gaussian distribution of signal noise [25].

## 2.3 ASELSAN INC.

The Aselsan group (C. Gozukara) computed the translational cases using ANSYS Fluent 15.0 [26], with an unstructured moving mesh composed of two zones; the outer grid surrounds an inner one, moving with the plate without going through a deformation. The outer zone is morphed and regenerated according to the predefined deformation rules to enable the inner zone to move. The mid-span cross-section grid slices are shown in Figure 2-3. Grids for RANS computations have 19426144 and 16767196 tetrahedral elements for translational surge and translational pitch cases, respectively. Slightly smaller grids are used for laminar computations. The domain is 80 *c* long, 40 *c* wide and 40 *c* high for the translational cases, and 60 *c* long, 40 *c* wide and 60 *c* for the pitching cases. The plate has a chord of 60 mm, thickness of 2 mm, and AR = 4. Reynolds number based on chord and terminal velocity is 3600 and 10,000, the former taken as laminar, and the latter run as RANS with a k-ε turbulence model [27]. One chord of travel is divided into 500 equal time steps for all cases. The initial conditions for the translational pitch cases are established by performing steady-state computations with zero angle of incidence.

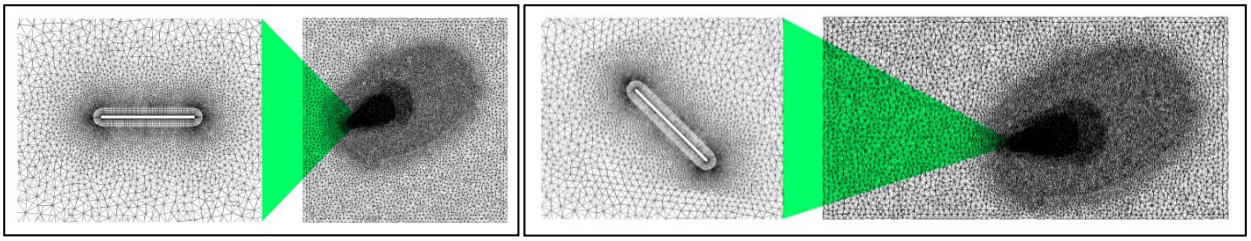

**Figure 2-3: Cross-Sectional View of Unstructured Mesh for Pitching (Left) and Surging (Right) Translations.**

## 2.4 CAMBRIDGE UNIVERSITY

The Cambridge University group (R. Stevens and H. Babinsky) performed experiments in the Cambridge Department of Engineering water towing tank (schematic in Figure 2-4). The tank has a 2 m long working section with clear side walls and floor for laser and camera optical access. The operational cross-section is 0.8 $m^2$. For an AR = 2 wing, maximum blockage (at $\alpha = 45°$) is 2.5%. A settling time between experiments of 20 minutes is deemed sufficient to achieve a quiescent fluid as determined by Jones [28]. The computer-controlled carriage on top of the tank can achieve a positional accuracy of +/-0.25%. Velocity is corrected for temperature variations greater than 1°C, giving a maximum error in freestream Reynolds number of O (1.25%).

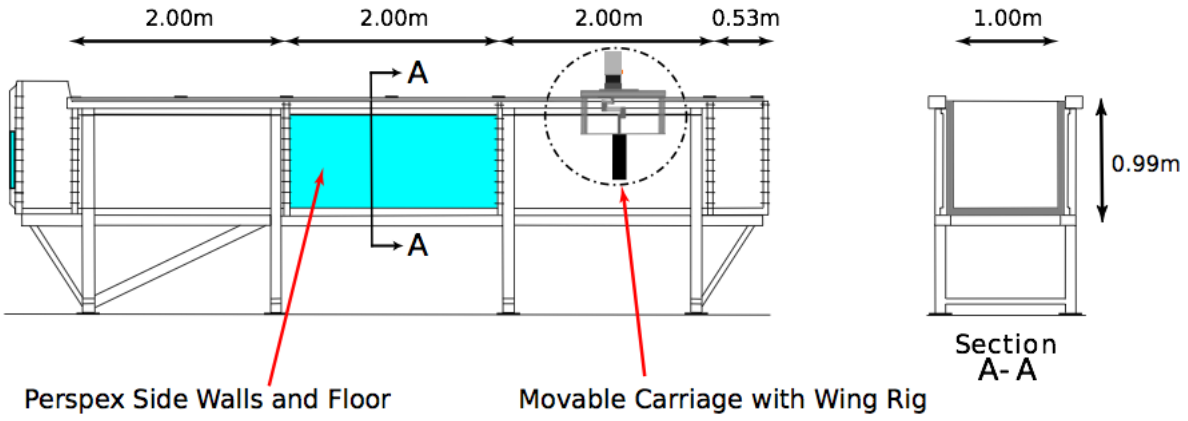


**Figure 2-4: Cambridge University Department of Engineering Tow Tank.**

The pitching rig (Figure 2-5) is used for both surging and pitching experiments. A skim plate is used to remove the influence of water free-surface effects and to act as a symmetry plane, giving an effective AR of twice the physical AR. Two different wings are used for experiments, one with a physical AR = 4 and one with AR = 2 (giving effective ARs of 8 and 4 respectively). For surging experiments the pitch motor is not activated and is fixed in place at the desired incidence. During pitching the wing incidence is verified using an algorithm based on the pixel illumination intensity of the wing reflection in PIV images and is accurate to within 3 – 4 pixels, giving a typical measured error over commanded incidence of less than 1 – 2 %.

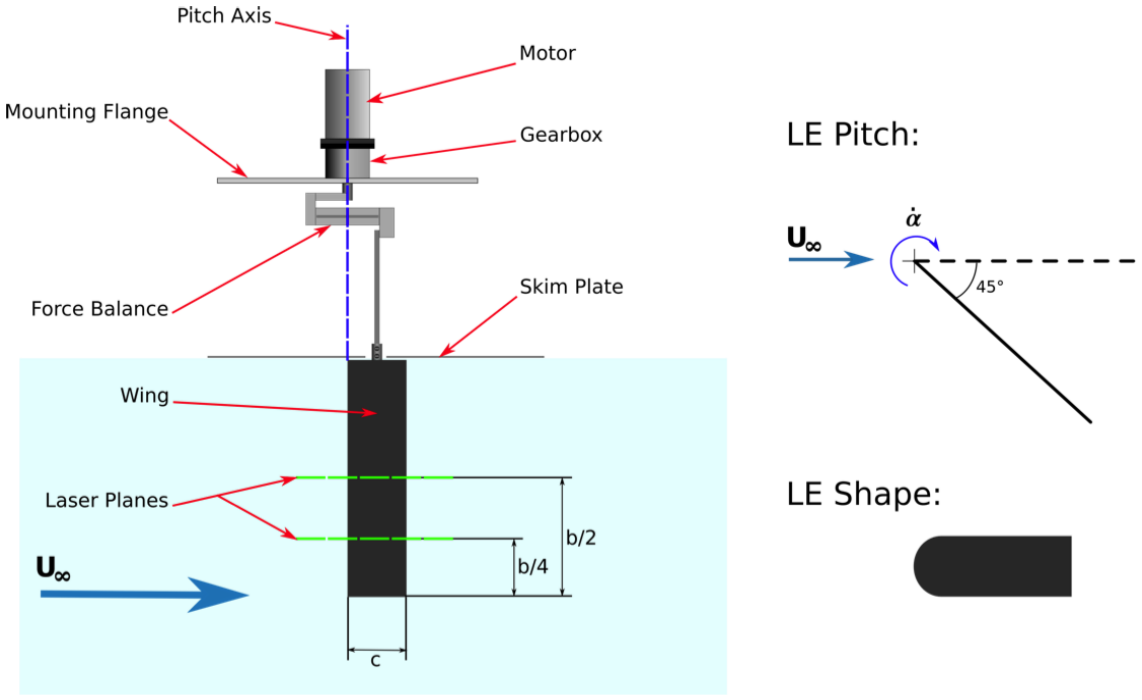


**Figure 2-5: Cambridge University Tow Tank, Model Installation Scheme.**

Lift and drag are measured with a force balance of the strain gauge load cell type. The two-component balance has a range of +/- 50 N and an accuracy within 0.01 N. Data is averaged over 10 runs, and smoothed using a moving-point average span of 100 data points with the endpoints treated by having progressively smaller span widths. The forces on the wing in air are also obtained and subtracted from the forces in water to remove the inertia force of the wing.

Dye flow visualization is performed using a dye composed of water and milk. Milk improves the stability of dye filaments, retarding diffusion of the filament into the main bulk of the fluid; milk also has the advantage of possessing good reflective properties [29]. A LaVision Flow Master planar PIV system uses $TiO_2$ particles for seeding, and camera with frame rate capability of more than 5 x $10^4$ Hz, at a resolution of 1024 x 1024 pixels. The field of view is 240 mm x 240 mm. Processing is with two passes of each interrogation window size, with windows decreasing from 32 x 32 to 16 x 16 pixels with Gaussian weighting and a 50% window overlap. Each vector represents an area of 1.6 x 1.6 $mm^2$ giving 75 vectors per chord length.

The $\gamma_2$ vortex detection scheme of Graftieaux *et al*. [9] is employed to identify the position of vortex cores in PIV data (contour centroid method). Using the LEV centre calculated by $\gamma_2$ as the epicentre, for each frame, a series of circular contours are defined with increasing radius. The circulation ($\Gamma$) around each contour is calculated and plotted with respect to contour radius. A best-fit Lamb-Oseen radial variation in $\Gamma$ (Eq. 2-1) is applied to the data, whence $\Gamma_{max}$ can be inferred. The calculated error in $\Gamma$ from the fit of a free Lamb-Oseen vortex is 0.23%:

$$\Gamma = \Gamma_{\infty}\left(1 - \exp\left(\frac{-r^2}{r_c^2}\right)\right) \qquad \text{(Eq. 2-1)}$$

r = radius of given contour.

$r_c$ = vortex core radius.

Equation n: Lamb-Oseen Circulation.

## 2.5 DLR

The German Aerospace Centre (DLR; H. Ehlers and R. Konrath), Institute for Aerodynamics and Flow Technology, performed Tomographic PIV experiments in the TU-Braunschweig wind tunnel, described below. Measurements capture phase-locked recordings (250 image pairs per chordwise position) of the flowfield above the moving wing for the 6 $c$ slow pitch case. A schematic of the measurement set-up is shown in Figure 2-6. Providing 400 mJ per pulse, a Nd:YAG laser (BigSky CFR) illuminates small DEHS tracer particles. The laser light volume was directed in a span-wise direction, with cross-section of $h \times t = 50 \times 20\ mm^2$. The width of the measurement domain was about 120 mm, starting 0.03 $b$ beyond the wing tip. Flow field data is not available between symmetry plane and $yn \approx 0.125\ b$ in span-wise direction. Four high resolution CMOS cameras (PCO.edge: $2560 \times 2160$ pixel, 16-bit) are arranged with two on each side of the test rig (Figure 2-6). A mirror was used to reflect the laser beam back, enhancing the scattered light intensity for the backward facing cameras. Due to the limited thickness of the laser volume, measurements had to be applied successively, scanning the flowfield in a chord-wise direction. The total measurement domain between leading and trailing edge consists of six sub-volumes. Tomo-PIV recordings have been taken for the time instances t* = 3 and 4.

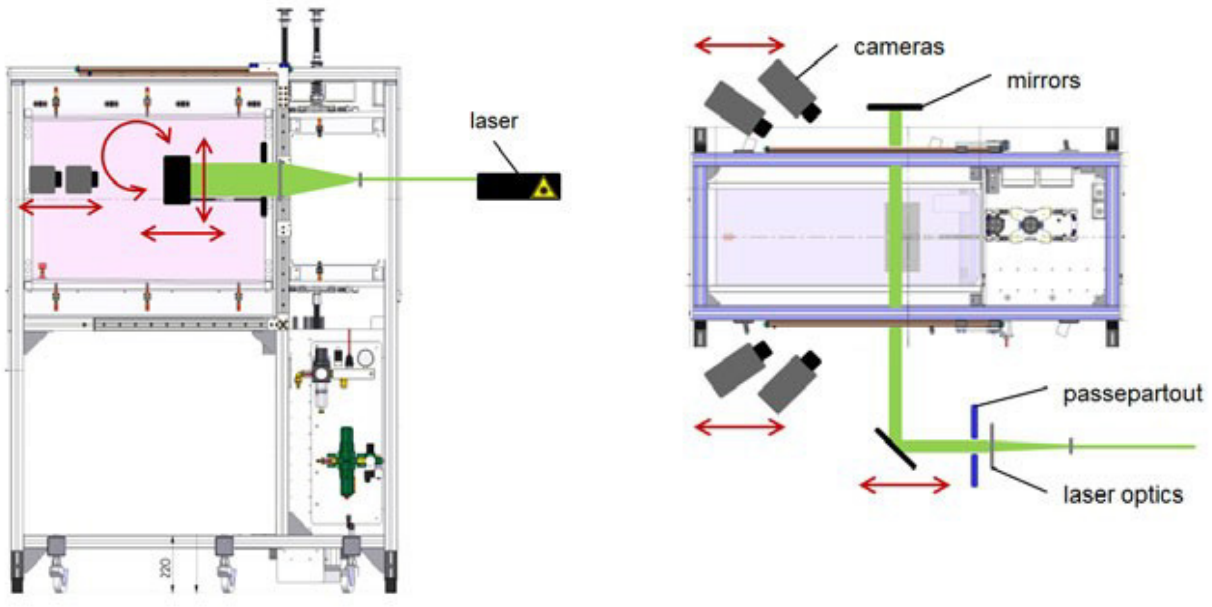


(a) (b)

**Figure 2-6: DLR Tomographic-PIV Optics Set-Up in TU-Braunschweig Wind Tunnel: Side View (a) and Top View (b).**

The data reduction procedure, using in-house software, is divided into three sub-routines: The camera calibration (which includes volume self-calibration), reconstruction of the particle distribution and a 3D cross-correlation routine. The reconstruction of the particle distributions was done using a SMART algorithm with MLOS initialization [30], [31]. The evaluation domain of every volume is represented by a voxel-space of 912 × 2177 × 329 voxel (resolution ≈ 18.2 voxel/mm). The voxel-to-pixel ratio was set to a value of 0.8, to allow an effective processing of the large amount of data. The recovered volume pairs of three-dimensional particle distributions are then processed with a cross-correlation-based displacement estimation algorithm. Just as in established 2-C processing schemes, the 3D algorithm employs a resolution pyramid which starts at a rather coarse grid and stepwise increases resolution while continually updating a predictor field. In the present application, a three level resolution pyramid was used with a final window size of $48^3$ voxel (75% overlap), resulting in vector volumes with 75 × 175 × 25 nodes. At this resolution volume deformation was applied twice using a cubic b-spline of order 3.

## 2.6 FLORIDA STATE UNIVERSITY

The Florida State University group (K. Taira and R. Jantzen) performed numerical simulations of translational pitch and surge using an immersed boundary method on a Cartesian Lagrangian grid [32], at sufficiently low Reynolds numbers so as to enable direct numerical simulation without sub-grid modeling or filtering. The spatial domain was discretized with a non-uniform Cartesian grid, with its spatial convergence verified. For pitching simulations, uniform flow was specified at the inlet and the plate was fixed at zero angle of attack to develop a laminar boundary layer. Once the boundary layer reached a steady-state, the pitching motion was initiated. For the surging simulation, the background flow was accelerated to match the experimental surging profile with the plate fixed on the grid. For the cases presented herein, the Reynolds number has been set to 300 based on the

translation and terminal velocity values for pitching and surging cases, respectively. The numerical solver and computational set-up have been verified and validated extensively, including flows over low-aspect-ratio plates [33] and comparisons with experiment [34]. A typical result, of 3D isometric visualization of vorticity contours for the AR = 4 surging plate, is given in Figure 2-7.

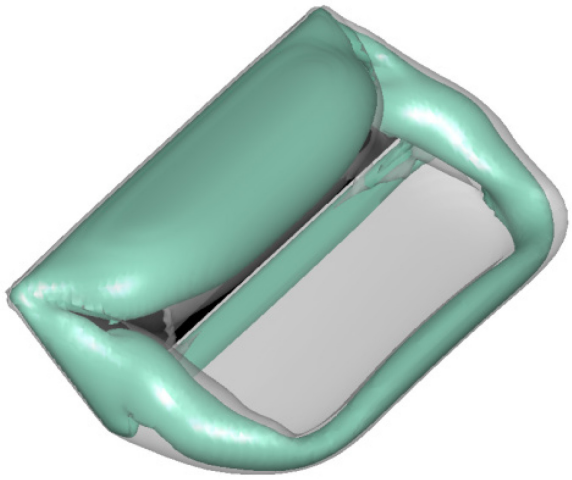

**Figure 2-7: Typical Results of Florida State University Immersed Boundary Method Solver, Contour Levels of Vorticity for the "Fast" AR = 4 Plate Surging in Translation.**

## 2.7 ISTANBUL TECHNICAL UNIVERSITY

Experiments by the Istanbul Technical University (ITU) group (O. Cetiner and O. Son) were performed in the close-circuit, free-surface, large-scale water channel located in the Trisonic Laboratories at the Faculty of Aeronautics and Astronautics of Istanbul Technical University. The cross-sectional dimensions of the main test section are 1010 mm × 790 mm. The models are mounted in a vertical cantilevered arrangement in the water channel about their leading edge as the pivot point. The connection rod connects the models to the servo motor from their leading edge to provide a ramp type pitch up motion via a coupling system. The chord length of the models is 10 cm and models have a span of 20, 30 or 40 cm to obtain different aspect ratios. The models are thin rectangular plates ($t$ = 0.5 cm) with sharp and round edges and they are manufactured of transparent Plexiglas® to allow laser light to illuminate both the suction and pressure sides. The experiments are conducted at a Reynolds number of 10,000 which corresponds to a flow speed of $U$ = 0.1 m/s.

Particle Image Velocimetry (PIV) technique is used to record flowfields around the models and therefore to analyze the vortical structures. The flow is illuminated by a dual cavity Nd:Yag laser (max. 120 mJ/pulse) and the water is seeded with silver coated hollow glass spheres with a mean diameter of 10 μm. Two 10-bit cameras with 1600 × 1200 pixels resolution are positioned underneath the water channel to capture the flow structures around the flat plate and in its near-wake. Two images from the two cameras are stitched before interrogation using two marker points in the illumination plane. Stitched PIV images are then interrogated using a double frame, cross-correlation technique with a window size of 64 × 64 pixels and 50% overlapping in each direction. The final grid resolution of velocity vectors is 3.5 mm × 3.5 mm in the plane of the flow. The resulting measurement plane is represented with approximately 3240 velocity vectors. The experimental set-up is shown in Figure 2-8.

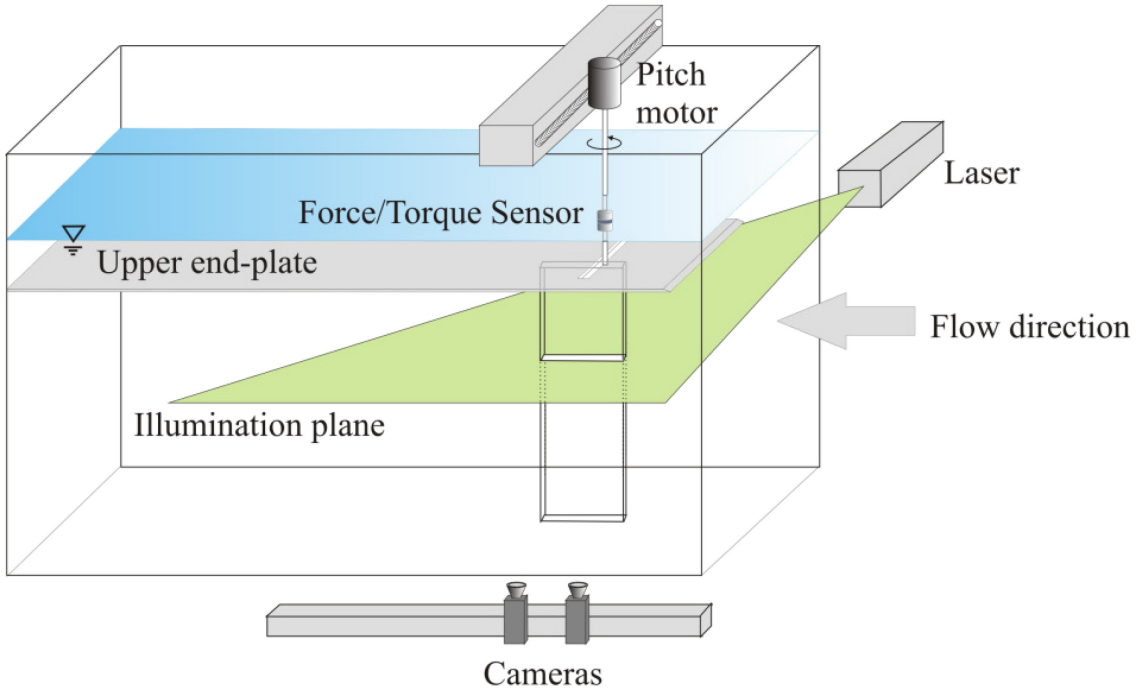


**Figure 2-8: ITU Experimental Set-Up.**

A six-component ATI NANO-17 IP68 Force/Torque (F/T) sensor [23] is used to measure the forces and moments acting on the model. The sensor is attached on the rod between the model and the pitch servo motor, oriented with its cylindrical z-axis normal to the pitch plane. The pitch-up motions of the airfoil are accomplished with a Kollmorgen/Danaher Motion AKM33E servo motor. The models are subjected to perform two types of motion: fast and slow. The model starts from 0° and reaches to its final angle of attack of 45° in 1 second for the fast motion and 6 seconds for the slow motion corresponding to 1 and 6 convective times respectively. Motor motion profiles are generated by a signal generator Labview VI (Virtual Instrument) for the given amplitude and duration. The same VI triggers both the force data acquisition and the PIV system. The force measurement starts 5 seconds before the beginning of the pitch motion; the synchronization with the PIV system is achieved using a National Instruments PCI-6601 timer device.

## 2.8 TECHNICAL UNIVERSITY OF BRAUNSCHWEIG

Experiments at the Technical University of Braunschweig (R. Radespiel and R. Wokoeck) were carried out in the LNB wind tunnel (Figure 2-9), a continuous Eiffel type tunnel with room recirculation designed to offer high quality flow with low perturbation. A typical turbulence level of $Tu < 0.1\%$ and a core velocity uniformity of 99% are achieved by a large nozzle contract ratio of 16 and several means of flow treatment and sound and vibration dampening.

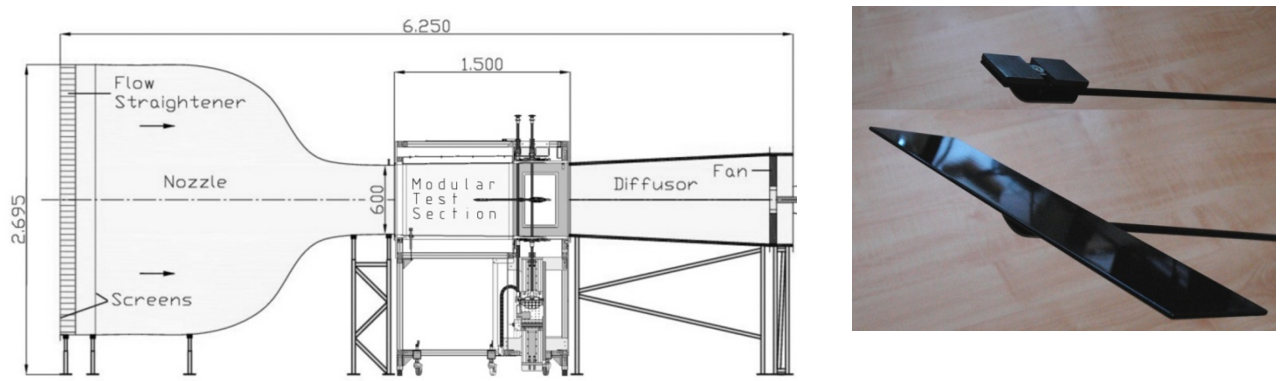


(a) (b)

**Figure 2-9: Wind Tunnel at TU-Braunschweig (a); Test Article and Inertial Dummy (b).**

The dynamic model support (Figure 2-9) is integrated into one of the 0.6 m high, 0.4 m wide and 1.5 m long modular test sections. To meet the required precision of high-speed flapping wing motions, it is driven by two linear direct electric motors, each delivering up to 700 N. The drives are controlled in a real-time closed loop with a 12-bit virtual cam resolution plus smooth interpolation and on the fly correction, with accuracy of ≤± 0.05 mm in vertical position and ≤± 0.1° angles of attack. Whilst the support is capable of carrying out pure plunging motions precisely, any motion containing a rotation portion is accompanied by a small unwanted horizontal translation.

Forces were measured with the 107 mm long and 11.2 mm in diameter six components internal strain gauge balance *W637*. Together with a *Hottinger Baldwin Messtechnik MGCplus* strain amplifier to process the balance signals, an accuracy of 0.015% of full scale is achieved. The full scale for the drag force is ± 7 N and for the normal force is ± 20 N, whilst the pitching moment may range up to ± 0.75 Nm. The force measurements are run through a 10 Hz low pass Bessel-filter to dampen out mechanical vibrations of the model support. The pitch moment is then referred to ¼ chord.

To separate the aerodynamic forces from the inertial forces, the latter are determined in a second measurement run with the wind tunnel off and an inertial dummy replacing the model. The dummy has to have the same mass, centre of mass and inertial moment in reference to the pitching axis as the model, but interacts much less with the air due to its compact, wingless design. Tuning the inertial dummy to the model values is an iterative process carried out with a fine weight balance, a tilting balance and a pendulum. The model was built by DLR in sandwich structure with layers of carbon fiber reinforced plastics around a foam core. The rectangular wing has fully round edges, a chord of 70 mm, a span of 280 mm and a thickness of 2.35 mm. Dummy and model as shown in Figure 2-9(b) both feature a body beneath the wing to cover the balance from wind and share a weight of 72.65 g.

## 2.9 TECHNICAL UNIVERSITY OF DELFT

The TU-Delft group (M. Percin and B.W. van Oudheusden) experiments were performed in a water tank at the Aerodynamics Laboratory of Delft University of Technology. The octagonal water tank (600 mm of diameter and 600 mm of height) is made of Plexiglas® allowing full optical access (Figure 2-10(a)). A Plexiglas® flat plate test-article has sharp edges, thickness of 3 mm, rectangular planform, length (*c*) of 50 mm, a span length (*b*)

of 100 mm, resulting in an aspect ratio of 2 (Figure 2-10(b)). The wing model was positioned at approximately 5 $c$ distance from the water surface, 7 $c$ distance from the bottom wall and 5 $c$ (wing tip to wall) distance from the side wall. A brushed DC motor with a gearbox (gear ratio of 132:1) connected to the main vertical axis ($y$ axis) of the set-up drove the wing in revolution, while pitch about the wing's leading edge ($z$ axis) was by a waterproof servo motor that was placed in the servo box which also contains the force sensor.

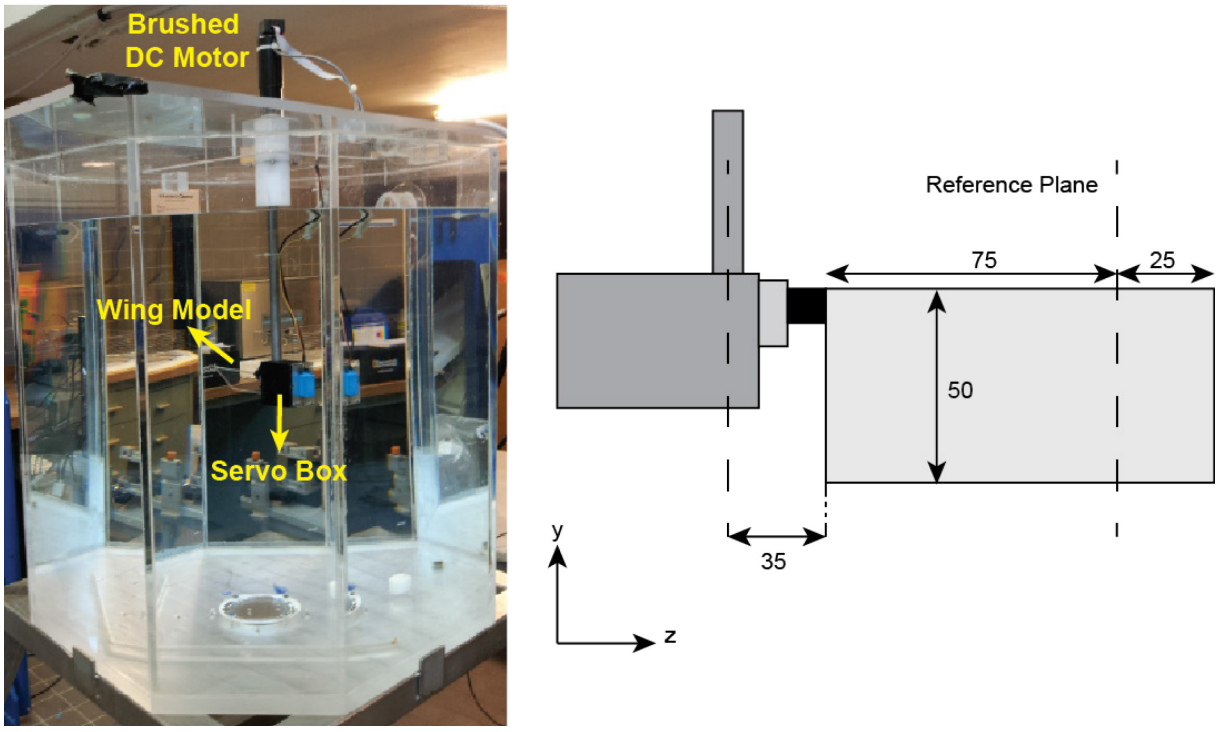


(a) (b)

**Figure 2-10: (a) Experimental Arrangement in the Water Tank; (b) Dimensions of the Wing Model.**

The distance between the root chord and the rotation axis is 35 mm (0.7 $c$) and the radius of gyration is $r$ = 90 mm, resulting in Rossby number of $r/c = 1.8$. The motion (Figure 2-11) is initiated by a constant acceleration from rest to $V_t = 0.2$ m/s (corresponding to the Reynolds number of 10,000 based on $c$) at an angle of attack ($\alpha$) of 0° over $\Delta t^* = 2$ ($\Delta s^* = 1$, corresponding to a revolution angle $\Delta\varphi = 25.8°$); this is then followed by a period in which the wing pitches up to $\alpha = 45°$ over $\Delta t^* = 1$ ($\Delta s^* = 1$) at a constant pitch rate, after which the wing continues to revolve at a constant rate at $\alpha = 45°$. On the other hand, in the revolving surge case (Figure 2-10(b)), the wing motion is initiated at $\alpha = 45°$ angle of attack with an acceleration period from rest to $V_t = 0.2$ m/s over $\Delta t^* = 2$ ($\Delta s^* = 1$) after which the wing remains to revolve at a constant angle of attack and constant rate. Note that for sake of comparison between the two cases, the origin for both the non-dimensional elapsed time ($t^* = 0$) and distance travelled ($s^* = 0$) are defined, such that they coincide with the start of the pitch/surge motion, respectively, with the terminal condition being reached at $s^* = 1$.

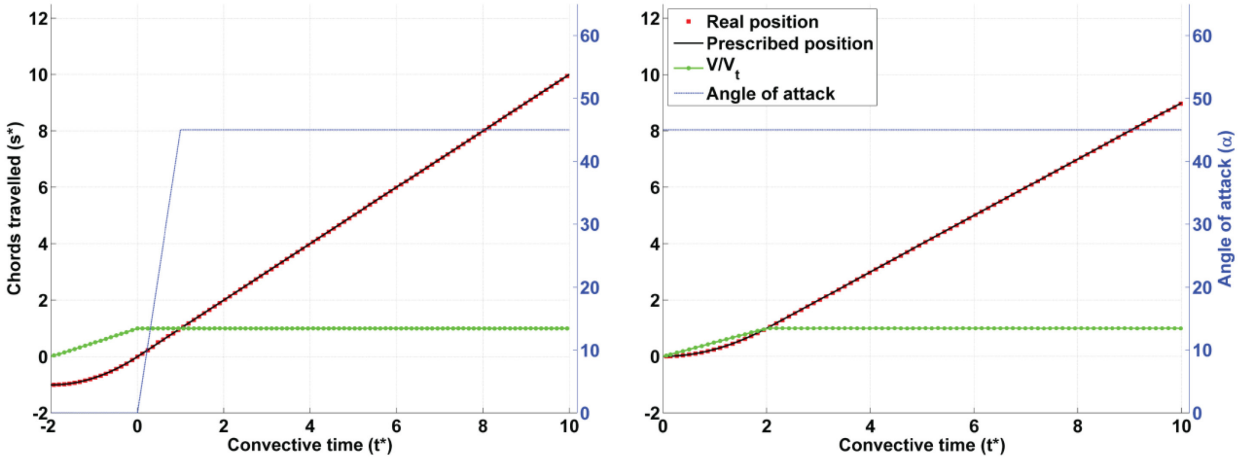


**Figure 2-11: Kinematics of the (a) Revolving-Pitching and (b) Revolving-Surging Motions.**

Real-time position and rotational velocity information was acquired from the motor encoder at 33 Hz data acquisition frequency to verify the actual motion kinematics. In all experiments, the entire travel distance is 14 $c$ ($s^* = 14$) corresponding to one full rotation. Although the forces were captured for the full motion, flowfield measurements were limited to the first 7 $c$ of travel.

Six components of forces and moments were measured with a water submergible ATI Nano17/IP68 force sensor. Force signals were acquired at 2 kHz data acquisition frequency via in-house developed LabVIEW code that also controls the motors and synchronizes the wing motion with the force data acquisition and the PIV measurements. Ensemble averaging of forces and moments was performed over 20 repetitions of the experiments for the pitching case and 50 repetitions for the surging case. The averaged force and moment data were then filtered to remove electrical noise and mechanical vibrations of the driving system as well as the natural frequency of the test rig (16.6 Hz) in the signal, by means of a Chebyshev Type II low-pass filter with a cut-off frequency of 15 Hz. A forward-backward filtering technique was used in order to prevent time-shift of the data. Lift and drag are normalized by use of the terminal velocity $V_t$ and wing surface area, in order to produce force coefficients ($c_L$ and $c_D$, respectively). The uncertainty in the reported force values were calculated based on the 15 Hz low-pass filtered signal which results in 0.5% and 1.5% average uncertainties with respect to steady-state mean values in the revolving-surging and revolving-pitching cases, respectively.

Three-dimensional quantitative information of the flow around the outboard section of the wing model was acquired via phase-locked Tomographic PIV [22]. At each run, a double-frame image was captured at a specific phase of the wing motion. Repeated runs were performed with sufficient time intervals to restore quiescent conditions in the water tank. The measurement volume of 90 × 70 × 25 mm$^3$ in size (Figure 2-12(a)) was positioned at two different spanwise locations side by side as shown in Figure 2-12(b). Then, a Kriging regression technique [35] with a correlating length of 2 mm in all directions was used in order to combine the two measurement volumes and to provide a complete visualization of the flowfield. The starting position of the wing was changed based on the desired measurement phase so to have the wing always oriented normal to the measurement volume during image acquisition. For each measurement phase, the experiments were repeated for three times and vector fields are ensemble-averaged in order to improve signal-to-noise ratio.

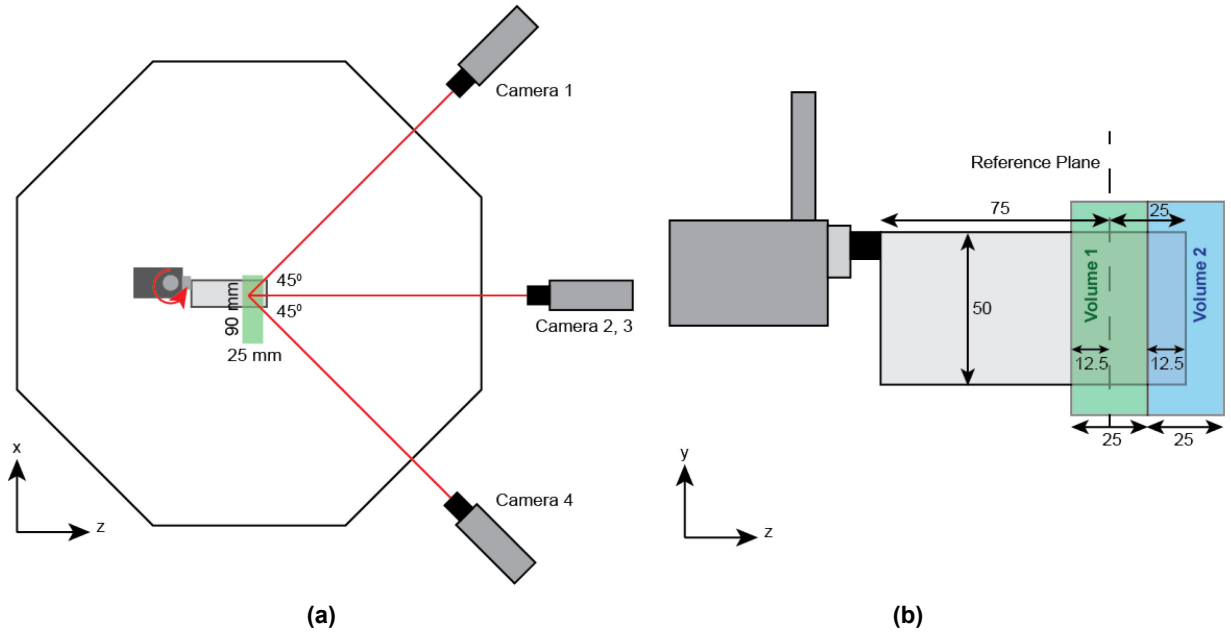


**Figure 2-12: (a) Sketch of the Top View of the Experimental Set-Up With Camera Arrangement; (b) Wing Model and Measurement Volume Arrangement.**

The volume was illuminated by a double-pulsed Nd:Yag laser at a wavelength of 532 nm. Polyamide spherical particles of 56 µm diameter were employed as tracer particles at a concentration of 0.4 particles/mm$^3$. The motion of tracer particles was captured by four 12-bit CCD cameras with a resolution of 1376 × 1040 pixels and a pixel pitch of 6.45 µm. Three cameras were arranged along different azimuthal directions in a horizontal plane while the fourth camera was positioned above the mid-camera in a vertical plane (Figure 2-12). Each camera was equipped with a Nikon 60 mm focal objective with numerical aperture f# = 11. Scheimpflug adapters were used on the three off-axis cameras to align the mid-plane of the measurement volume with the focal plane. The digital resolution is 15 pixels/mm and the average particle image density is approximately 0.04 particles per pixel (ppp). Image pre-processing, volume calibration, self-calibration, reconstruction, and three-dimensional cross-correlation based interrogation were performed in LaVision DaVis 8.1.5. The measurement volume was calibrated by scanning a plate with 9 × 10 dots through the volume in depth of 25 mm with steps of 5 mm. In each calibration plane, the relation between the physical coordinates and image coordinates is described by a 3$^{rd}$-order polynomial fit. Linear interpolation is then used to find corresponding image coordinates at intermediate z locations. Image pre-processing with background intensity removal, particle intensity normalization and a Gaussian smooth with 3 × 3 kernel size was performed in order to improve the volume reconstruction process. Particle images were interrogated using windows of final size 32 × 32 × 32 voxels with an overlap factor of 50%. The resultant vector spacing is 1.0 mm (0.02 $c$) in each direction, forming a dataset of 87 × 68 × 24 velocity vectors in the measurement volume.

## 2.10 WROCLAW UNIVERSITY OF TECHNOLOGY

The Wroclaw University of Technology group (H. Kudela and T. Kozlowski) computed the translational-cases (pitch and surge) in 2D, using an in-house vortex-in-cell method for the incompressible Navier-Stokes equations. Casting the Navier-Stokes into stream-function-vorticity form, one obtains a Helmholz equation, which was solved using a viscous splitting algorithm [36], [37], [38]. First, the inviscid equation is solved:

$$\frac{\partial \omega}{\partial t} + u\frac{\partial \omega}{\partial x} + \upsilon\frac{\partial \omega}{\partial y} = 0 \qquad \text{(Eq. 2-2)}$$

and then, the viscous one (Stokes problem):

$$\frac{\partial \omega}{\partial t} = \nu\Delta\omega\,,\ \omega(\mathbf{x}, 0) = \omega, \omega|_{\partial\Omega} = \omega_b \qquad \text{(Eq. 2-3)}$$

From the inviscid equation, the vorticity is constant along characteristics, yielding a system of ordinary differential equations once the domain is discretized over a mesh. The mesh is used to solve the Poisson equation for stream function. Initial vorticity field is replaced by a discrete distribution of vortex particles that are placed in nodes of the grid, with a circulation assigned to each particle. Particles' circulation changes in time due to diffusion.

To simplify mesh definition, the flat-plate with rounded edges was replaced with an ellipse of fineness ratio 50.

## 2.11 UNIVERSITY OF BUFFALO

The University of Buffalo group (M.J. Ringuette, Z.R. Carr and A.C. DeVoria) experiments were done at the Vortex Dynamics & Bio-Inspired Propulsion Lab at the State University of New York at Buffalo [39], [40]. The facility is a 91 cm × 77 cm × 71 cm glass tank with a 50% by mass glycerin-water mixture; the density and viscosity are 1130.5 kg/m$^3$ and 5.78 × 10$^{-3}$ Ns/m$^2$.

The configuration is a rectangular squared-edged flat-plate wing rotating from rest with a 45° incidence. Figure 2-13(a) shows the wing-aligned coordinates. The velocity program, driven by a motion controller, is a symmetric-in-time trapezoid (Figure 2-13(a) inset, green line); the position error is at most 0.03°. Acceleration/ deceleration occur over the first/last 10° of rotation; the total rotation is $\phi_{final}$ = 120°. For force measurements, the motion is smoothed during acceleration using a hyperbolic tangent curve (purple line) with the same average angular acceleration. While numerous variants were run, the parameter-set closest to the AVT-202 canonical rotational surge case has: AR = 2, t/c = 0.053, root cut-out 0.14 *c*, Re (based on span) of 10,000; this is for the PIV data set. Forces were taken with root cut-out of 0.30 *c*, Re 2000 – 10,000. Following Harbig *et al*. [45], we use a span-based Reynolds number, $Re_{span} = U_{tip}b/\nu$. Acceleration occurs over ~ 0.3 *c* at 75% span (0.25 *b* inboard of the tip).

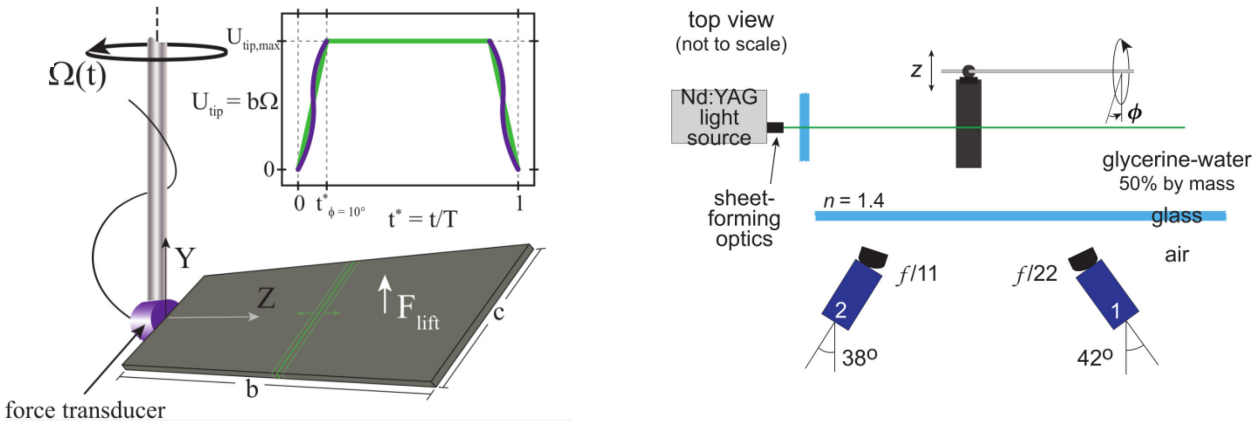


(a) (b)

**Figure 2-13: (a) Wing Coordinates, Laser Sheet Orientation, and Velocity Program; (b) S-DPIV Set-Up Schematic.**

The S-DPIV data are acquired via an approximately symmetrical angular camera arrangement (Figure 2-13(b)). Volumetric velocity fields are reconstructed from phase-locked, phase-averaged S-DPIV in multiple, closely-spaced constant-span planes. The wing is incrementally translated between runs along the span ($z$-direction), normal to the laser sheet. The out-of-plane spatial resolution is 0.06 $c$ (0.08 $c$) for AR = 2 (AR = 4), with an in-plane resolution twice as fine. Angular positions are acquired at $\phi = 6°–120°$ with $\Delta\phi = 6°$. The in-plane velocity uncertainty is ~ 0.01 $U_{tip}$; it is about twice this out-of-plane. For AR = 2 and 4, the final velocity fields are obtained by phase averaging 5 and 7 fields, respectively. The force transducer is a submersible ATI Nano 17-IP68 attached at the wing base (Figure 2-13(a)). The sampling frequency is 1 kHz and 40 runs are averaged for each case. The uncertainty from static tests is 0.63% of the measurement for forces of $O(1)$ N. After averaging, low-pass filtering mitigates noise and mechanical vibrations.

## 2.12 UNIVERSITY OF CALGARY

The University of Calgary group (D. Rival and J. Kriegseis) performed experiments in a Rolling Hills free-surface water tunnel. Plunging and surging motions for an AR = 4 plate were controlled by a custom hexapod manipulator (see Figure 2-14). The flow was interrogated with three-dimensional particle-tracking velocimetry (3D-PTV). To obtain particle tracks, the tunnel was seeded with neutrally buoyant 100 µm silver-coated, hollow glass spheres with a Stokes number of Stk = 1.2 x $10^{-3}$, and illuminated by a High-Intensity Discharge (HID) light source. A lens system (40 and 300 mm converging lenses) collimated the light to provide a measurement volume with a diameter of 100 mm. The plates were painted black to prevent light scattering. Raw images were recorded with four pco.edge sCMOS cameras (chip size 2560 x 2160 pixels, maximal resolution of 2560 x 1280 pixels at 165 frames per second). Direct force measurements were recorded by means of an ATI Gamma [23] six-component force/moment sensor, which was located between the base of the hexapod and the sting holding the plate. The plate had a chord length of $c$ = 50 mm, a span of 4 $c$ = 200 mm and t/c = 6%. Based on the chord length and free stream velocity U or the final towing speed h(dot) = 0.1 m/s (depending on the case), the Reynolds number was set to Re = 5000. Note that the coordinates' point of origin is placed at the intersection of the leading edge and the tip edge. To identify the influence of initial conditions on vortex formation and orientation, as well as the circulation and overall force history, different plate kinematics were applied to the AR = 4 flat plate.

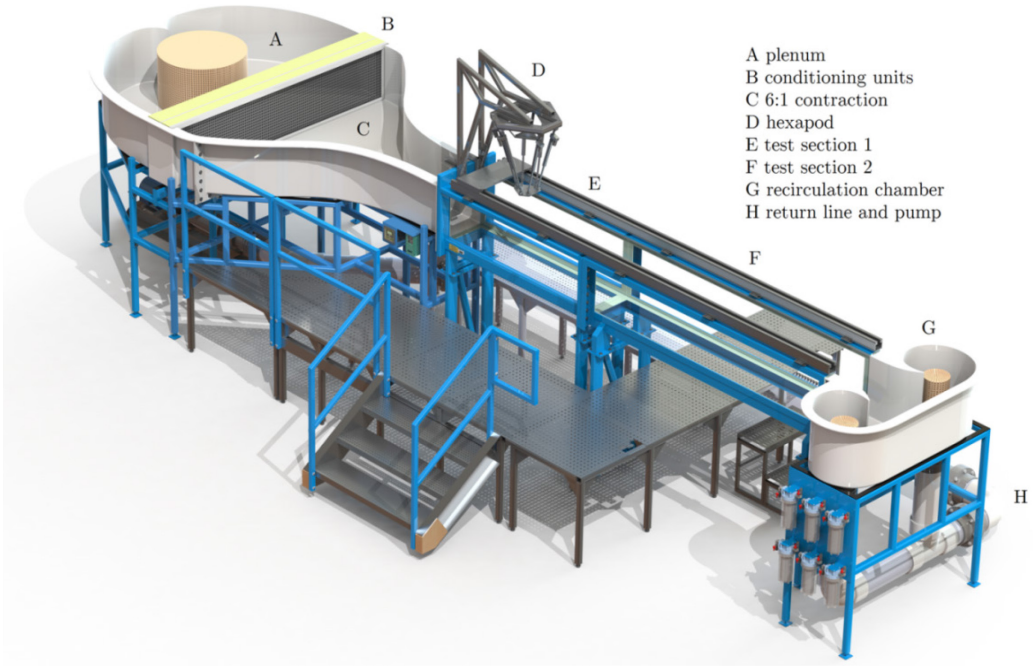


**Figure 2-14: University of Calgary Free-Surface Water Tunnel and Hexapod Rig.**

## 2.13 UNIVERSITY OF MARYLAND

The Maryland group (A. Jones, P. Mancini and F. Manar) performed experiments in the 7 m x 1.5 m x 1 m tow tank (Figure 2-15) at the University of Maryland, and in the AFRL water tunnel (the latter is discussed above).

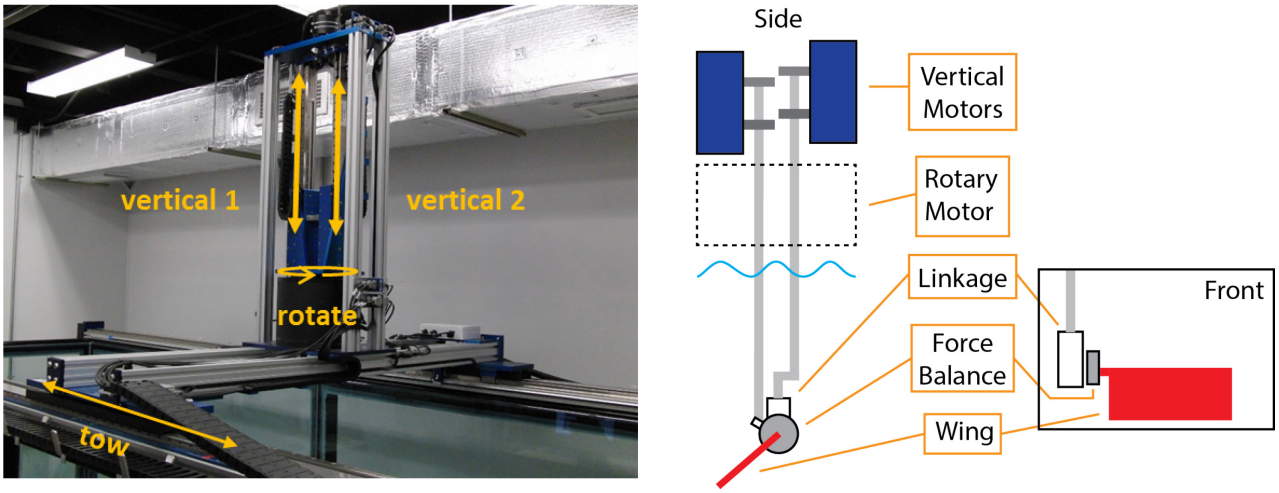


(a) (b)

**Figure 2-15: University of Maryland Towing Tank: Photograph of Electric Motors Atop of Tank (a) and Schematic of Rotating/Pitching Wing Actuation (b).**

The towing tank is equipped with a 4-axis motion control. The motor assembly, shown in Figure 2-15(a), is mounted on the towing carriage, and contains two brushless linear motors, a direct-drive brushless rotary stage, model supports, and a slip ring to transfer power and other signals to/from the equipment on the rotary stage. Vertical plunge (± 49 cm) and pitch (± 90 deg.) are driven by the two linear motors and a custom-designed Hoeken linkage. Continuous rotation is provided by the rotary stage. Carriage translation (7 m) is directly driven by a pair of brushless linear motors. All stages are equipped with optical encoders, and the entire traverse system is controlled using a multi-axis Galil motion controller to within 0.1 mm. Pitch motion is accurate to within 0.1 degrees. After each test, the motion of the fluid was observed to come to a standstill after about 3 minutes. To ensure absolute quiescent conditions, 5 minutes were allowed to pass between each test run.

An ATI Mini40 6-axis force/torque transducer with force resolution of 0.01 N and a torque resolution of 0.0001 Nm was used for direct loads measurement. The sampling rate was 1000 Hz. Each case was run 5 times, starting from different locations in the tank. Starting at a slightly different location served to help average out noise from any bumps in the carriage travel. Results were then averaged. The load cell was fixed to the pitch linkage with a 3D-printed adapter plate. Another 3D-printed adapter is used to fix the wing directly to the force balance; the force balance therefore collected data directly in the wing frame. To isolate only the fluid loads, the contributions from gravity and buoyancy were removed from the measured force. In the surge cases, the average force over the first second was taken as the net gravity and buoyancy force and subtracted from the measurement. For the pitch cases, the tare process is slightly trickier because of the changing direction of gravity in the force balance frame. To remedy this, forces were taken with a static wing at angles of attack ranging from -60 to 60 degrees in 15 degree increments. These static forces were fit with a 3$^{rd}$-degree polynomial in angle of attack, which was used to tare the gravity and buoyancy forces at any angle of attack. Inertial loads were measured in air and the magnitude of the resulting force was found to be negligible.

The forces were smoothed in time with MATLAB's 'smooth' function using the "lowess" option with a width set to 0.5 chords of travel at the final velocity, which corresponds to 0.25 seconds in real time. The "lowess" option creates a least squares quadratic fit over the smoothing window for each point in the original data set and evaluates the resulting quadratic polynomial at the point in question. This method does a good job of rejecting noise without introducing a phase shift, while still accurately capturing the magnitude of peaks in the data.

For all cases in this facility, the wing was an AR = 2 flat plate with a chord of 100 mm and slightly rounded edges**,** and thickness of 0.08 inches**.** For the rotation case, the root cut-out was 0.5 *c*, and the angular velocity was set to achieve the same velocity as the translating case at 75% of the tip radius from the axis of rotation. Put another way, the radius of 1.875 chords from the axis of rotation was used to compute the Reynolds number and to normalize the forces. The surge cases were run at a fixed incidence of 45 degrees, and the pitch cases were pitched from 0 degrees to 45 degrees.

Both translation and rotation velocity profiles were computed using the "Eldredge function" [7] with a smoothing parameter, *a*, of 24. The pitch kinematics used the Eldredge function as a position profile. The fast pitching case used a smoothing parameter of 15, and the slow case used 4. For rotational pitch, the wing was set to 0 degrees and then accelerated to the final velocity and moved through 5 chords of travel before beginning the pitch motion.

## 2.14 UNIVERSITY OF MICHIGAN

The Michigan group (H-T. Yu and L. Bernal) performed experiments in a free-surface water tunnel at the Department of Aerospace Engineering (Figure 2-16). The tests section is 0.6 cm x 0.6 cm x 2 m. The free-stream velocity is controlled using an AC induction motor, which is calibrated as a function of test section water

depth using PIV. The flow speed ranges from 5 cm/s to 40 cm/s and the free stream turbulence intensity is below 1%. The model wings were made of Plexiglas®, $c$ = 2", t = 0.125", for t/c = 0.0625, with all edges rounded. They are immersed in water for a 2-chord span, resulting in physical AR = 2 and effective AR = 4, taking the water surface as a symmetry plane.

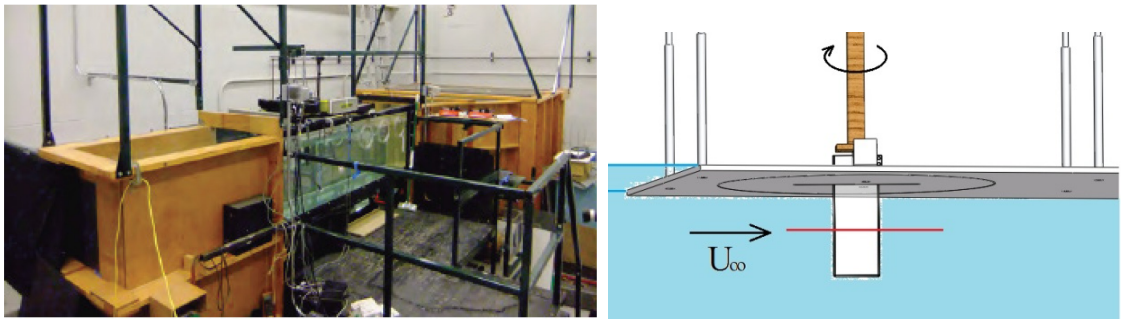


**Figure 2-16: University of Michigan, Department of Aerospace Engineering Low-Turbulence Free-Surface Water Tunnel. Left: photograph of facility; Right: schematic of AR = 2 plate suspended vertically underneath a free-surface skimmer plate.**

The wing motion is the usual linear pitch ramp from 0° to 45° with Eldredge [7] smoothing at the start and the end of the ramp. Several values of the smoothing parameter were used [41]. A Velmex Rotary Table model B4832TS and stepper motor RK266-03 are used for the wing motion. The kinematics is discretized with 13 points at every smoothed region. For all measurements the motion is repeated 60 times, and phase-averaged. For details, see Yu *et al*. [42] and Yu and Bernal [43].

Forces are measured via an ATI Nano-43 load cell [23]. The sensor center is on the pitch axis and the sensor axes are aligned with the chord direction, plate normal direction and span direction, respectively. The sensor's maximum calibrated load is 18 N, and the resolution is 1/256 N, in all three axes. Both the force sensor and the rotary table are located above the water surface. The wings are attached to the tool side of the sensor with an aluminum adapter designed to minimize the mass of the model. Data processing includes low-pass filter and tare. The low-pass filter is a zero-phase first-order two-pass Butterworth, with cut-off frequency was determined by Fourier analysis of the motion acceleration to retain 90% of motion spectral content. A dynamic tare consisted of repeating the exact same motion in both water and air, and subtracting the results. No static calibration was needed because of the small mass of the model and the excellent alignment of the span axis with the vertical direction.

Flow visualization was conducted using a dye rake (7 probes with 1" spacing), two syringe pumps, and two different color dyes (i.e., blue and red). The injection rake was placed at 50 % of wing span. Since the density of the dyes (ESCO Foods) is 1012 kg/m$^3$, they were mixed with alcohol to match the water density, 998 kg/m$^3$. Images were recorded using Nikon D3100 camera at a frame rate of 30 Hz.

Conventional 2D PIV and lens-shifted Stereo PIV were used. The lens-shifted Stereo PIV system was developed specifically for this research [41]. In a typical test, the magnification was 13 pix/mm and the particle displacement between images approximately 8 pix. PIV images were processed using in-house developed MATLAB software, which uses a cross-correlation algorithm to determine the particle displacement with sub-pixel resolution, and a two-pass algorithm.